THE JOURNAL OF PHYSICAL CHEMISTRY LETTERS
A JOURNAL OF THE AMERICAN CHEMICAL SOCIETY

pubs.acs.org/JPCL Letter

Curvature Engineering of SiFe Dual-Atom Catalysts for Enhanced CO_2 Electroreduction

Meijie Wang, Yuxing Lin, Yaowei Xiang, Yang Sun, Zi-zhong Zhu, Shunqing Wu, and Xinrui Cao*

Cite This: J. Phys. Chem. Lett. 2026, 17, 1227−1234 Read Online

ACCESS | Metrics & More | Article Recommendations | Supporting Information

ABSTRACT: Geometric tuning of supports is an emerging strategy to optimize catalysts, yet its role in governing the synergy of heteronuclear p−d dual-atom catalysts (DACs) is unexplored. Using carbon nanotubes (CNTs) as tunable curvature substrates, we investigated their influence on $SiFeN_6$ DACs via first-principles calculations. We reveal an inverted-volcano-type relationship between curvature and activity, originating from the nonlinear differential response of key intermediates. This curvature-driven trend is a general principle applicable to other 3d transition metals (TM = Mn, Co, Ni). To rationalize this complex relationship, we integrated a machine learning (SISSO) approach, which yielded a robust multidimensional descriptor (R^2 = 0.92). By quantitatively revealing the dominant role of the p-block Si site, our data-driven model establishes substrate geometry as a primary and effective design strategy for optimizing these complex dual-atom catalysts.

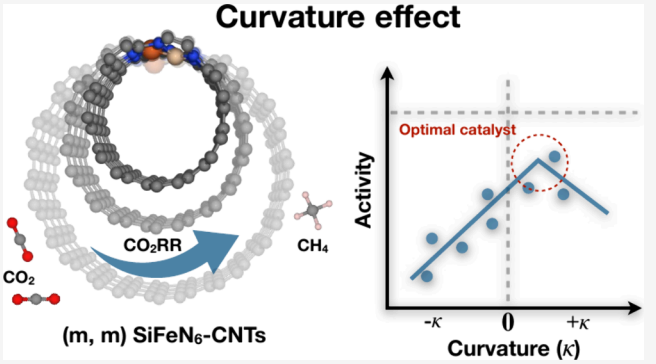

The escalating concentration of atmospheric carbon dioxide (CO_2) due to anthropogenic activities presents a profound global challenge, necessitating urgent and innovative strategies for carbon mitigation and utilization.[1,2] The electrochemical CO_2 reduction reaction (CO_2RR), powered by renewable electricity, has emerged as a cornerstone technology for a sustainable future, offering a direct pathway to convert this greenhouse gas into valuable fuels and chemical feedstocks, such as carbon monoxide (CO), formic acid (HCOOH), and hydrocarbons.[3−5] However, realizing a circular carbon economy hinges on the development of electrocatalysts with exceptional activity, outstanding product selectivity, and long-term stability under industrial conditions. Despite significant progress, current catalysts often suffer from large overpotentials, poor selectivity toward high-value multielectron products, and rapid deactivation, which collectively hinder the economic viability of CO_2RR technologies.[6,7]

The development of atomically dispersed catalysts has progressed from traditional nanoparticles to well-defined single-atom sites,[8,9] which have already demonstrated remarkable activity and selectivity across many reactions. These single-atom catalysts (SACs) have provided a powerful platform for establishing mechanistic principles and metal−ligand electronic interactions.[10] Building on this foundation, dual-atom catalysts (DACs) have recently emerged as a complementary class of systems in which two adjacent metal centers can offer additional degrees of freedom—such as metal−metal cooperation, multielectron activation, and tunable reaction pathways.[11,12] To date, optimization of DACs has primarily focused on active site engineering,[13,14] which typically involves screening various elemental combinations to identify the most intrinsically active pairs. Indeed, our previous study highlighted SiFe as a promising DACs candidate for CO_2RR, underscoring the potential of p−d heteronuclear motifs.[15,16] However, beyond this initial coarse-tuning of elemental composition, further enhancing catalytic performance requires more subtle, fine-tuning strategies. Recently, a purely physical tuning knob—the support's intrinsic geometric curvature—has emerged as a distinct and powerful new strategy.[17−24] Yet, predominantly curvature studies to date focus on transition metal SACs and DACs, neglecting heteronuclear p−d synergies. How curvature governs the unique synergistic mechanism between a p-block element and a transition metal, such as in the SiFe moiety, for promoting the complex CO_2RR has not yet been investigated.

Herein, to bridge this critical knowledge gap, we employ systematic density functional theory (DFT) calculations to investigate how curvature governs the catalytic performance of the heteronuclear p−d dual-atom catalyst, $SiFeN_6$, for the CO_2RR. We used armchair carbon nanotubes (CNTs) as geometrically well-controlled supports, constructing a series of (m,m) CNTs with chirality indices m ranging from 4 to 13 to

Received: December 11, 2025
Revised: January 5, 2026
Accepted: January 14, 2026
Published: January 20, 2026

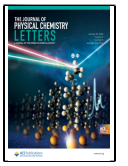

https://doi.org/10.1021/acs.jpclett.5c03896
J. Phys. Chem. Lett. 2026, 17, 1227−1234

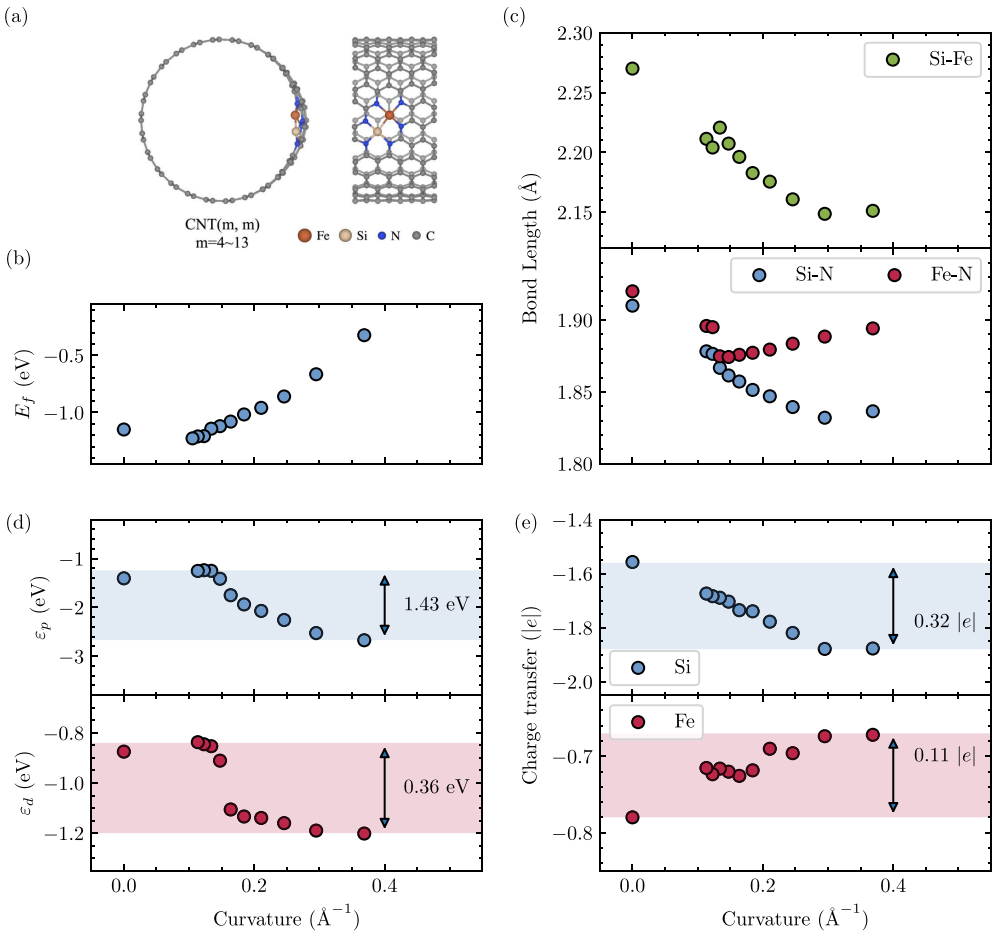

Figure 1. (a) Structural model. (b–e) Properties versus curvature (κ): (b) Formation energy (E_f); (c) Key bond lengths; (d) Fe d-band center (ε_d) and Si p-band center (ε_p); (e) Bader charge transfer.

provide ten distinct and tunable curvatures (Figure 1(a)). The corresponding curvature and diameter values for each (m,m) CNTs are summarized in Table S1. The planar $SiFeN_6$-graphene (Figure S2) is adopted as the zero-curvature benchmark. Its structural stability and electronic characteristics have been systematically established in our previous studies,[15] providing a reliable foundation for evaluating curvature-induced effects. Although the global geometries of CNTs differ from other curved carbons, the local curvature-induced electronic features they generate are highly similar, making CNTs a representative model for probing curvature effects. It is noteworthy that CNTs with moderate curvatures within our studied range (e.g., m = 7–10, corresponding to diameters of 1.0–1.4 nm) are among the most commonly synthesized, adding practical significance to our investigation.[25] Our findings reveal that curvature acts as a primary performance descriptor, leading to an inverted-volcano-type relationship between curvature and catalytic activity. We further establish the generality of this principle and, finally, employ SISSO to extract interpretable multidimensional descriptors that capture complex electronic structure–property relationships where traditional models fall short, highlighting their utility in guiding catalyst design.

First, the stability of the catalysts, a prerequisite for their practical application, was evaluated by calculating the formation energies (Figure 1(b)). The considered catalysts are thermodynamically stable. The $SiFeN_6$-graphene exhibits a formation energy of −1.15 eV, while the values for $SiFeN_6$-CNTs range from −1.23 to −0.32 eV as curvature increases. This indicates that while low-curvature nanotubes are slightly more stable than the planar sheet, higher curvature generally reduces stability. Even so, the extremely curved (m = 4) CNT exhibits substantial strain energy (Figure S3(a)) yet still supports a dynamically stable SiFe DAC. *Ab-initio* molecular dynamics simulations further verify that the active site and carbon framework remain intact under such high curvature (Figure S3(b)). Curvature also tunes the active site bonding environment (Figure 1(c)). Compared to the planar configuration (Si–Fe: 2.27 Å; Si–N: 1.91 Å; Fe–N: 1.92 Å), increasing curvature leads to a distinct bond contraction: the Si–Fe and Si–N bonds shorten to 2.22–2.15 Å and 1.88–1.83 Å, respectively. In contrast, the Fe–N bond exhibits a nonmonotonic trend: it initially contracts from the planar value 1.92 Å to 1.87 Å in low-curvature nanotubes, but then slightly elongates to 1.90 Å as curvature further increases. These observations suggest that geometric curvature promotes stronger in-plane Si–Fe interation, which concurrently reinforces the Si–N bonds.

The curvature of the carbon support induces a significant redistribution of the catalyst's electronic structure. This is primarily driven by geometric strain, which increases with curvature and promotes a shift from an sp^2 to a slight sp^3-like character in the carbon framework. Then, states near the Fermi level become progressively more localized at higher curvatures,

https://doi.org/10.1021/acs.jpclett.5c03896
J. Phys. Chem. Lett. 2026, 17, 1227–1234

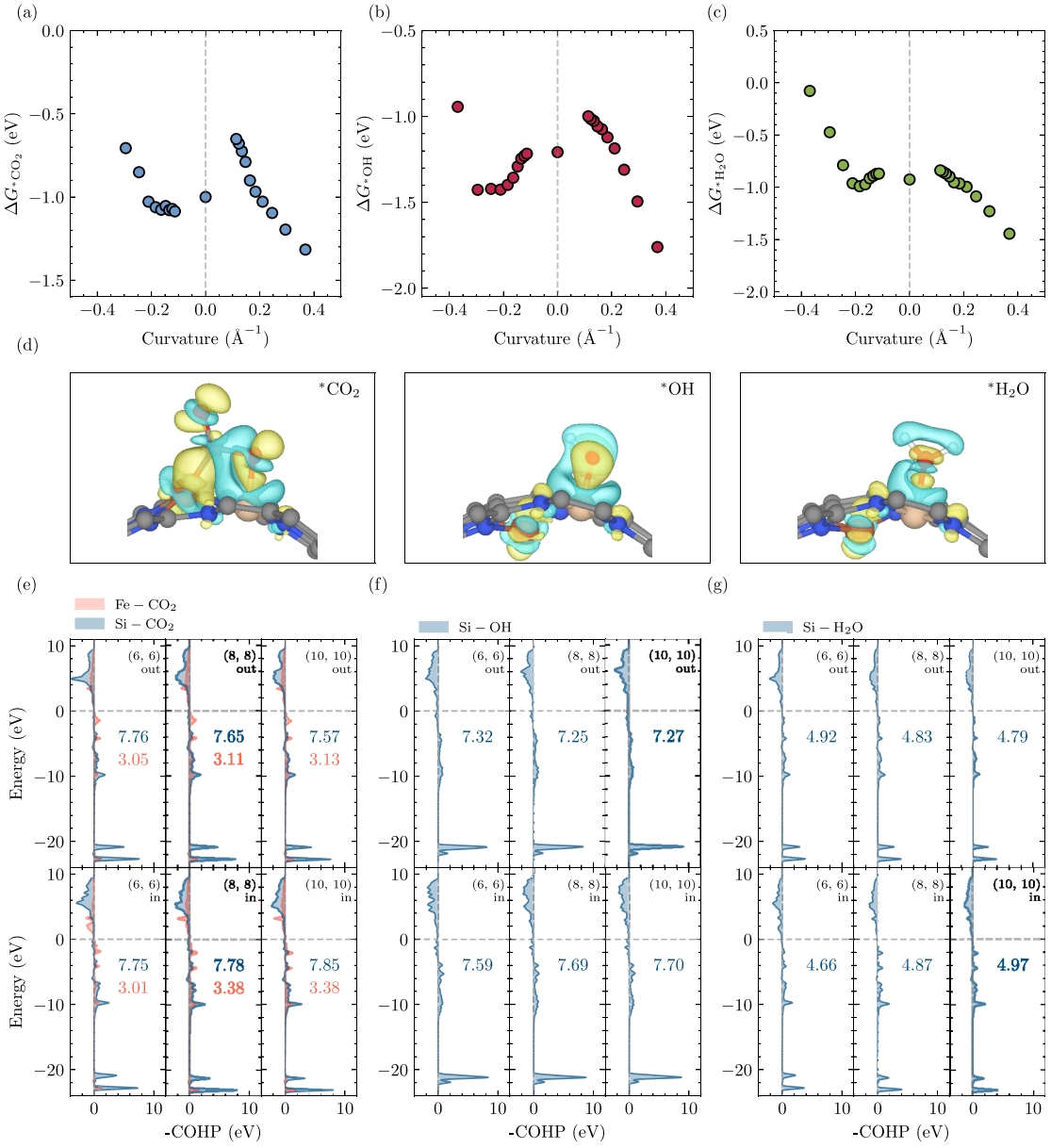

Figure 2. Adsorption free energies for (a) *CO_2 (ΔG_{*CO_2}), (b) *OH (ΔG_{*OH}) and (c) *H_2O (ΔG_{*H_2O}). (d) Representative charge density difference plots for the adsorption of *CO_2, *OH and *H_2O on the m = 10 exterior surface (isosurface value = 0.005 |e|/Å^3; yellow/cyan denotes charge accumulation/depletion). (e–g) Projected Crystal Orbital Hamilton Population (-ICOHP) plots for the key adsorbate–substrate bonds upon adsorption of (e) *CO_2, (f) *OH, and (g) *H_2O on representative SiFeN$_6$–CNTs. The −ICOHP values represent the integrated COHP up to the Fermi level, with larger magnitudes corresponding to stronger bonding interactions.

in contrast to the delocalized π-system of the low-curvature limit (Figure S4). Furthermore, with increasing curvature, both the Fe d-band (ε_d) and Si p-band (ε_p) shift downward in energy. The Si ε_p is particularly sensitive to this geometric modulation, varying by approximately 1.43 eV, far exceeding the shift of the Fe ε_d (0.36 eV). Alongside these band shifts, we observe that the Si-p–Fe-d orbital overlap integral ($S_{overlap} = \int_{-\infty}^{+\infty} \min(\rho_{Fe_d}(E), \rho_{Si_p}(E))\, dE$), used here as a measure of p–d coupling strength, exhibits a nonmonotonic dependence on curvature, first increasing at moderate curvature and then decreasing at higher curvature (Figure S5). These results indicate that curvature not only shifts the individual band centers of Si and Fe, but also modulates the strength of p–d hybridization between them. Bader charge analysis (Figure 1(e)) also reveals pronounced charge transfer effects. The electron loss from the Si atom is substantially enhanced (from 1.56 to 1.88 |e|), while it is modestly suppressed for the Fe atom (from 0.78 to 0.67 |e|), leading to a more electropositive Si site. Furthermore, the total magnetic moment of the SiFeN$_6$-CNTs remains nearly constant at ∼2.0 μ_B across the entire curvature range (Table S2). As a representative example, the spin density of the (9,9) SiFeN$_6$-CNT shows that the spin polarization is predominantly localized around the Fe center (Figure S6). Together with the constrained spin calculations confirming this configuration as the thermodynamic ground state for the highly curved (m = 4) case (Figure S7). These results suggest that the magnetic state of the SiFe active site is robust against geometric distortion. Collectively, these electronic modifications demonstrate that curvature is an

https://doi.org/10.1021/acs.jpclett.5c03896
J. Phys. Chem. Lett. 2026, 17, 1227–1234

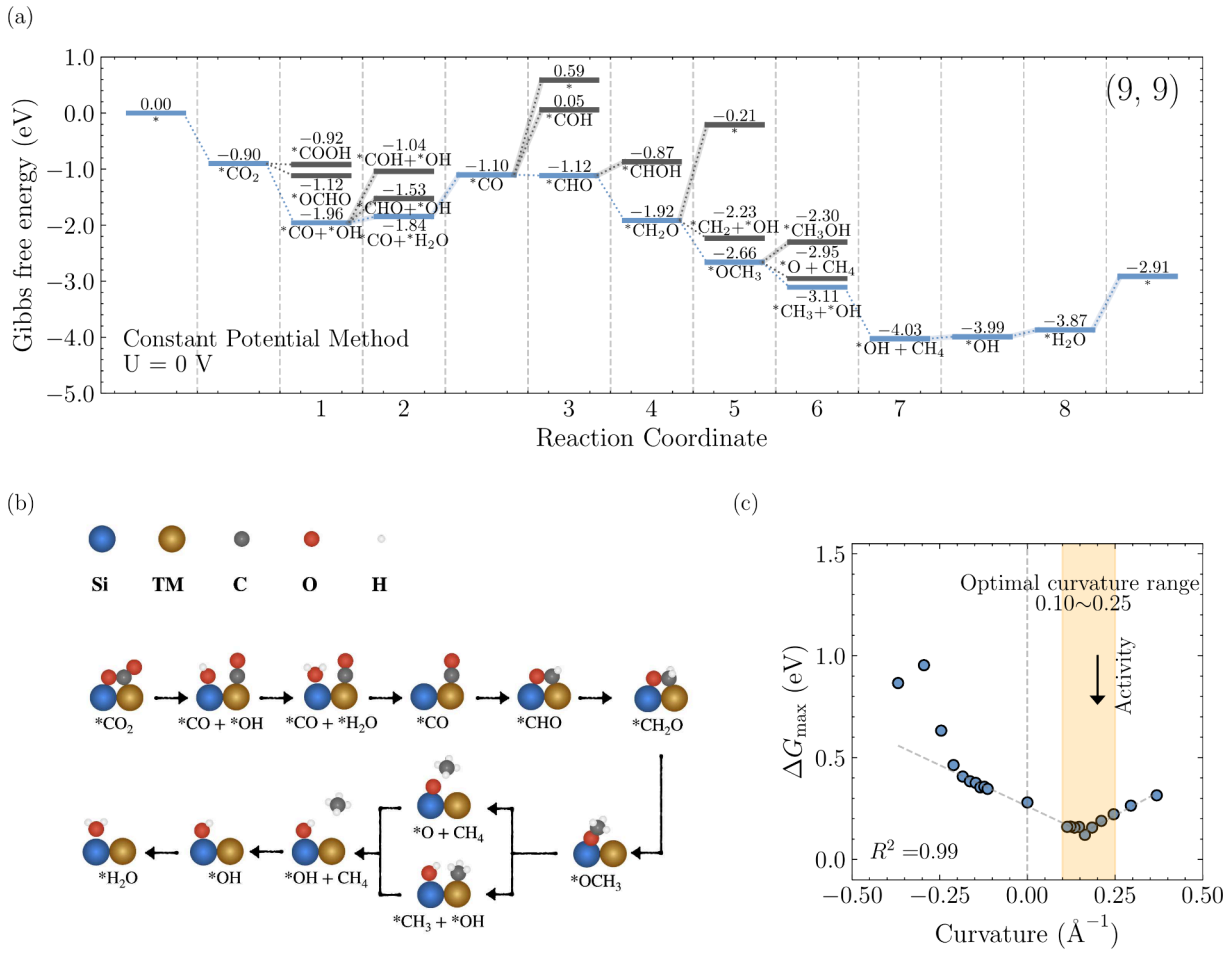

Figure 3. (a) Free-energy step diagrams for exterior adsorption on (9,9) $SiFeN_6$-CNT; (b) Computationally determined optimal reaction pathway for CO_2RR on $SiTMN_6$-CNTs; (c) The reaction energy of RDS (ΔG_{max}) versus curvature (κ). The linear fitting excludes data points with $\kappa < -0.2$.

effective tool for tuning the catalyst's electronic properties, with the Si site acting as the more responsive component. We next examine how these changes impact the catalytic performance for the CO_2RR.

The overall efficiency of the CO_2RR is governed by two fundamental factors: the initial activation of the CO_2 molecule and the thermodynamics of the subsequent proton-coupled electron transfer (PCET) steps, among which the terminal *OH → $*H_2O$ transformation frequently represents the most crucial bottleneck for Si-based DACs. Therefore, the binding strengths of $*CO_2$, *OH, and $*H_2O$ serve as essential descriptors for predicting the catalytic activity of CO_2RR. Consequently, we have performed a systematic investigation into the adsorption behavior of these three key species on the $SiFeN_6$-CNTs surfaces. Consistent with our previous work,[15,16] we modeled $*CO_2$ in its stable bidentate configuration (O−Si, C−Fe), while both *OH and $*H_2O$ were modeled in their preferred on-top Si site.

Given the complex environment within carbon nanotubes, we first performed a set of control calculations to isolate the effects of the concave interior, independent of the embedded $SiFeN_6$ active site. We calculated the adsorption energies of CO_2, CO, and H_2 along the central axis of pristine CNTs with varying diameters (Figures S8 and S9(a)). As shown in Figure S9(a), the adsorption energies for all three molecules exhibit a clear inverted-volcano-type relationship with curvature: the interaction strengthens with decreasing negative curvature before weakening dramatically under high confinement. To illustrate this extreme confinement effect, we focus on the (4,4)-$SiFeN_6$ system—the smallest-radius structure in our study—where the charge density difference plot for an internally adsorbed $*CO_2$ molecule reveals direct electronic interaction with the opposing nanotube wall (Figure S9(b)), a clear signature of severe confinement. Accordingly, while the key adsorption energetics for the interior sites will be presented for completeness, our in-depth electronic structure analyses will henceforth focus on the exterior surface, which holds greater relevance for practical catalysis.

The curvature-dependent adsorption free energies of $*CO_2$ (ΔG_{*CO_2}), *OH (ΔG_{*OH}) and $*H_2O$ (ΔG_{*H_2O}) on the $SiFeN_6$-CNTs are shown in Figure 2(a-c). The planar $SiFeN_6$-graphene system (curvature $\kappa = 0$) serves as a reference state. These trends are primarily governed by a delicate interplay between local electronic modulation at the active site and geometric confinement effects, with the dominant factor shifting as a function of curvature. In the positive curvature regime (convex surface), local electronic modulation is the decisive factor. The adsorption of $*CO_2$, *OH, and $*H_2O$ strengthens with increasing positive curvature, with adsorption energies ranging from −0.65 to −1.32, −1.00 to −1.76, and −0.84 to −1.45 eV, respectively. This trend is fully consistent with our preceding electronic structure analysis, which showed that higher curvature induces greater charge loss from the Si site. This renders the Si atom more electropositive, thereby

https://doi.org/10.1021/acs.jpclett.5c03896
J. Phys. Chem. Lett. 2026, 17, 1227−1234

promoting stronger electrostatic and bonding interactions with the oxygen-containing adsorbates. Under negative curvature (concave surface), the adsorption behavior is codetermined by the electronic structure of the active site and geometric confinement effects. In the low-to-moderate negative curvature regime (> −0.20 $Å^{-1}$), the interplay of these factors leads to divergent trends among the adsorbates: $*CO_2$ adsorption slightly weakens (from −1.09 to −1.03 eV), $*H_2O$ adsorption shows minor strengthening (from −0.87 to −0.96 eV), while *OH binding is markedly enhanced (from −1.22 to −1.43 eV). However, at highly negative curvatures, the geometric confinement effect appears to become dominant, resulting in a sharp destabilization for all intermediates. Importantly, the curvature-induced interplay between local electronic modulation and geometric confinement leads to the differential evolution of the binding strengths of the rate-determining step (RDS) relevant intermediates (*OH and $*H_2O$), which is a critical factor in modulating the overall catalytic activity.

To deconstruct the key adsorbate-site interactions at an electronic and bonding level, we combined charge density difference (CDD) (Figure 2(d)) and Crystal Orbital Hamilton Population (COHP) analyses[26,27] (Figure 2(e−g)). CDD plots, exemplified by the m = 10 exterior surface, visually reveal significant charge redistribution between the $SiFeN_6$ moiety and the adsorbates ($*CO_2$, *OH and $*H_2O$). To quantitatively understand the nature of these interactions, we further calculated the integrated COHP (-ICOHP) values for the key chemical bonds. For $*CO_2$ adsorption, the -ICOHP value for the Si-CO_2 bond (from 7.57 to 7.85 eV) is substantially larger than that for the Fe-CO_2 bond (from 3.05 to 3.38 eV), directly corroborating the dominant role of the Si site in the initial activation of CO_2 from a bond-strength perspective. Consistently, Bader charge analysis (Table S3) shows that Si experiences a much larger charge redistribution (−0.89 to −0.77 |e|) upon $*CO_2$ adsorption compared with Fe (−0.03 to 0.05 |e|), further confirming its dominant electronic role in activating CO_2. PDOS analysis (Figure S10) also reveals stronger Si p-state hybridization with O p-states in the bonding region (−3 to −8 eV), fully consistent with the much larger −ICOHP values of the Si−adsorbate bonds. It is worth noting that, in the early stage of CO_2 activation, the Fe site dominates: one O atom first binds to Fe, after which cooperative Fe−C and Si−O interactions stabilize the activated CO_2 (Figure S11). Furthermore, the Si−OH bond (from 7.25 to 7.70 eV) is significantly stronger than the Si−H_2O bond (from 4.66 to 4.97 eV). This difference in bond strength not only accounts for their markedly different sensitivities to surface curvature but also explains the high energy change for *OH removal on the Si site. Intriguingly, the relationship between bond strength and overall adsorption energy diverges dramatically between the exterior and interior surfaces. On the exterior, the calculated −ICOHP values show a strong correlation with the adsorption energy trends. In stark contrast, the inner surface exhibits a paradoxical behavior: as the internal curvature decreases (m increases), all bond strengths uniformly increase, a trend that is diametrically opposed to the weakening adsorption energy observed for *OH and $*H_2O$. This decoupling of local bond strength from overall adsorption stability underscores the complexity of the interior environment and highlights the dominant role of other factors.

Building on the adsorption analysis, we investigated the full CO_2RR catalytic cycle to assess curvature's effect on activity. Free energy profiles of the C_1 pathway were computed for both interior and exterior surfaces (Figures 3(a), S12 and S13). The active-site geometry and preferred adsorption motifs remain unchanged across all curvatures, except for interior adsorption in the highly curved m = 4 system, where strong concave confinement induces noticeable deviations. Overall, the variation in reaction energetics is governed primarily by curvature-induced electronic modulation and geometric confinement rather than by structural or configurational changes. Although curvature can perturb the reaction pathway, the CH_4 route (Figure 3(b)) remains the most favorable for all systems except for interior adsorption in the extremely curved m = 4 structure. Importantly, the final PCET step, $*OH + H^+ + e^- \rightarrow *H_2O$, is the RDS for all $SiFeN_6$-CNTs. Strong *OH binding on the Si site makes its removal as H_2O difficult, slowing the reaction rate. Furthermore, we correlated curvature (κ) with the RDS free energy (ΔG_{max}), a vital activity descriptor where smaller values reflect superior catalytic performance. As depicted in Figure 3(c), the reaction energy of this RDS is highly sensitive to the substrate's curvature. A clear inverted-volcano relationship emerges between catalytic activity and curvature, with the optimal performance found at m = 9 (0.16 $Å^{-1}$). Notably, catalytic activity remains consistently high across a broader curvature window of approximately 0.10−0.25 $Å^{-1}$, indicating a relatively tolerant optimal regime. At this curvature, the $SiFeN_6$−CNTs exhibit the lowest free energy change for the rate-determining step (ΔG_{max} = 0.12 eV), significantly outperforming both the planar graphene benchmark (ΔG_{max} = 0.28 eV) and other curvatures. This inverted-volcano trend arises from the disparate effects of curvature on the adsorption of the reactant (*OH) and product ($*H_2O$). As established previously, their respective adsorption free energies (ΔG_{*OH} and ΔG_{*H_2O}) shift at differential rates as curvature changes. Consequently, the free energy of the RDS ($\Delta G_{max} = \Delta G_{*H_2O} - \Delta G_{*OH}$) is minimized at this moderate curvature. Interestingly, ΔG_{max} exhibits a linear correlation with the Si-p−Fe-d orbital overlap integral ($S_{overlap}$), despite the rate-determining step occurring at the Si top site (Figure S14). This correlation suggests that the curvature-dependent p−d coupling provides an additional electronic handle that accompanies the modulation of the Si p-band, reinforcing the role of Fe in dynamically tuning the reactivity of the Si center and mitigating excessive *OH binding. To examine the robustness of this curvature−activity relationship under realistic reaction conditions, additional constant-potential calculations were performed at a representative CO_2RR potential of −1.0 V vs RHE for two selected cases, namely the structure with optimal curvature (m = 9) and that with extreme curvature (m = 4). As shown in Figure S15, applying −1.0 V mainly results in significantly enhances $*CO_2$ adsorption and lowers the energy of all hydrogenation steps. Importantly, the RDS and relative activity ordering between the two structures remains unchanged. Furthermore, energetic analysis indicates that the outer surface generally exhibits superior catalytic activity. Due to its spatial configuration, the outer surface is inherently more exposed to the reaction environment and electrolyte, resulting in higher active site accessibility. Consequently, the reduction process is expected to occur predominantly on the exterior surface of the catalyst.

We also considered the selectivity by evaluating the competitive adsorption of $*CO_2$ versus $*H_2O$. As shown in Figure S16, surfaces with a positive curvature in the range of 0.18 to 0.25 $Å^{-1}$ exhibit favorable selectivity toward CO_2

https://doi.org/10.1021/acs.jpclett.5c03896
J. Phys. Chem. Lett. 2026, 17, 1227−1234

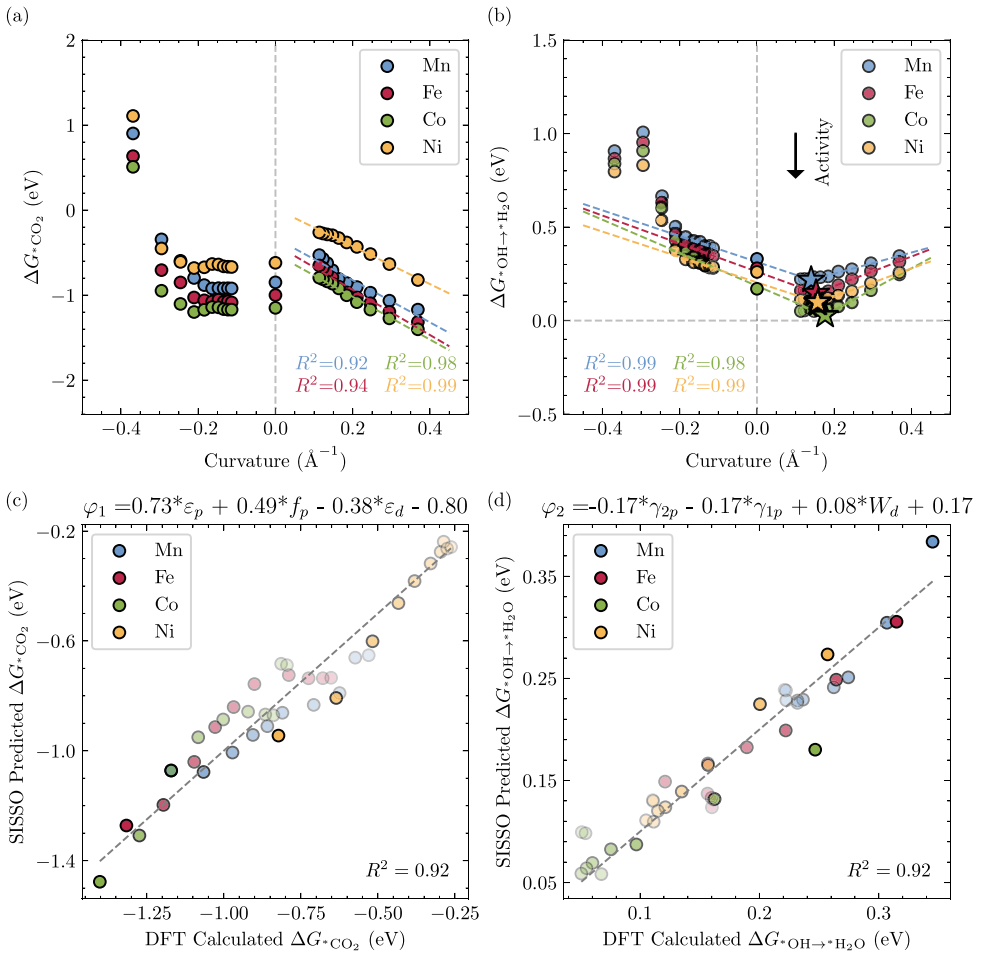

Figure 4. Generality of curvature as a catalytic descriptor and performance validation of the SISSO machine learning model. (a) Free energy of $*CO_2$ adsorption (ΔG_{*CO_2}) as a function of curvature (κ) for $SiTMN_6$−CNTs with TM = Mn, Fe, Co, and Ni. (b) Reaction energy of the possible rate-determining step ($\Delta G_{*\,OH\rightarrow *H_2O}$) as a function of curvature (κ) for the same systems; the pentagrams indicate the optimal points of the inverted-volcano trends. (c) Parity plot comparing DFT-calculated vs SISSO-predicted values for the $*CO_2$ adsorption free energy (ΔG_{*CO_2}). (d) Parity plot comparing DFT-calculated vs SISSO-predicted values for the possible RDS reaction energy ($\Delta G_{*\,OH\rightarrow *H_2O}$). Points in panels (c) and (d) are rendered with curvature-dependent transparency, where more transparent markers correspond to smaller curvature values.

activation. For the concave surfaces, most structures also show good selectivity, except for the highly strained (4,4) tube, where selectivity is compromised by the onset of severe steric and electronic confinement. In addition, the consideration of an external potential further optimizes this selectivity; as demonstrated by our constant-potential analysis, the applied potential of −1.0 V vs RHE significantly strengthens $*CO_2$ binding while concurrently weakening the adsorption of $*H_2O$. In summary, curvature significantly regulates both the activity and selectivity of the $SiFeN_6$−CNTs for CO_2RR. A slightly convex surface supporting the Si−Fe diatomic pair affords the best catalytic activity and selectivity.

To validate the hypothesis that curvature tuning is a general principle for catalytic design, we extended our investigation beyond the SiFe system to include other 3d transition metals (TM = Mn, Co, Ni) in the $SiTMN_6$−CNTs framework. We first examined CO_2 adsorption and observed highly consistent trends across all systems (Figure 4(a)). On exterior surfaces, adsorption strengthens with increasing curvature for the considered TMs. Conversely, on interior surfaces, all systems exhibit slight weakening at moderate curvatures, followed by a sharp drop under high-confinement conditions. Crucially, this geometric control of adsorption translates directly to the overall catalytic activity. As shown in Figure 4(b), the RDS reaction energy for all investigated systems (TM = Mn, Fe, Co, Ni) follows a similar, distinct inverted-volcano relationship with curvature. Although the absolute activity varies with the TM identity, the overarching activity trend is conserved. For SiCo, which shows pronounced activity in the range of 0.10−0.25 Å^{-1}, the ΔG_{max} is confined to a narrow window of 0.05−0.10 eV. These results convincingly demonstrate that substrate curvature acts as a primary performance descriptor, governing the catalytic activity of these SiTM DACs regardless of the specific transition metal. This establishes geometric tuning not merely as a viable method, but as a robust and overarching strategy for catalyst optimization.

While electronic descriptors such as the TM d-band center (ε_d) and Si-centered descriptors including the p-band center (ε_p) or the p−d orbital overlap integral ($S_{overlap}$) can capture adsorption trends within a given $SiTMN_6$−CNT system as the curvature varies, their predictive power deteriorates when different SiTM species are considered collectively, where cooperative p−d interactions and metal-specific responses lead to distinct, metal-dependent scaling relations rather than a

https://doi.org/10.1021/acs.jpclett.5c03896
J. Phys. Chem. Lett. 2026, 17, 1227−1234

universal trend. As shown in Figure S17, these single-feature descriptors fail to establish a correlation for the adsorption and reaction energies on the exterior surfaces of the different SiTM-CNTs. This breakdown of conventional models highlights the necessity for multidimensional descriptors that can capture the complex interplay between the active site's electronics and the substrate curvature. To this end, we employed the Sure Independence Screening and Sparsifying Operator (SISSO) method[28] to identify compact, physically interpretable descriptors for adsorption and activity (see Supporting Information for details). The resulting descriptors exhibit excellent predictive performance (Figure 4(c−d)), which is further validated by leave-one-out cross-validation (Figure S19; R^2_{CV} = 0.90 for φ_1 and 0.89 for φ_2). For *CO_2 adsorption, the optimal descriptor (φ_1, R^2 = 0.92) $\varphi_1 = 0.73\varepsilon_p + 0.49\ f_p - 0.38\varepsilon_d - 0.80$ is fully consistent with the underlying electronic structure. The strong positive coefficients of the Si p-band center (ε_p) and p-band filling (f_p) indicate that higher and more populated Si 3p states weaken their interaction with the O atoms of CO_2. An upward shift of the Si p-band center reduces the contribution of deep Si−O bonding states to the hybridization with CO_2, while an increased Si 3p occupation enhances the population of Si−O antibonding states. Both effects weaken the overall bond strength, in full agreement with the PDOS and COHP analysis. In contrast, the negative coefficient of the Fe d-band center ($-0.38\varepsilon_d$) shows that a higher ε_d, i.e., closer to the Fermi level, strengthens adsorption, in line with the d-band−center model: a raised ε_d pushes antibonding states upward, reduces their occupation, and reinforces bonding. The relative coefficient magnitudes further confirm that Si plays the dominant role in CO_2 activation. For catalytic activity (ΔG*OH→ *H_2O), the second descriptor (φ_2, R^2 = 0.92) $\varphi_2 = -0.17\gamma_{2p} - 0.17\gamma_{1p} + 0.08\ W_d + 0.17$ shows that activity is governed mainly by how the Si 3p DOS shape responds to curvature. The negative coefficients of the kurtosis (γ_{2p}) and skewness (γ_{1p}) indicate that sharper and more asymmetric p-band profiles lower ΔG by modifying the adsorption energies of both *OH and *H_2O, with the underlying electronic-structure changes affecting the two intermediates to different extents. A more localized, shallower-energy 3p DOS preferentially weakens *OH binding (relative to *H_2O), which facilitates its removal and lowers ΔG. The small positive coefficient of the Fe d-bandwidth (W_d) suggests a minor modulation through enhanced Fe−Si electronic coupling that influences the OH/H_2O adsorption balance.

In summary, this work systematically elucidates the profound impact of substrate curvature as a precise tuning knob for CO_2RR performance, using $SiFeN_6$−CNTs as a model system. This work demonstrates that curvature modulates the electronic structure of the p-block Si site to a significantly greater extent than the d-block Fe site. The differential evolution of the binding strengths of the RDS reactant (*OH) and product (*H_2O) as a function of curvature gives rise to an inverted-volcano-type relationship between geometry and catalytic activity. Furthermore, we establish the generality of this principle by extending our investigation to other transition metals (TM = Mn, Co, Ni). The discovery that the inverted-volcano activity trend is a universal feature confirms that geometric tuning is a broadly applicable design strategy capable of modulating performance regardless of the intrinsic properties of the TM. Finally, by employing the SISSO machine learning method, we successfully developed robust, multidimensional descriptors that accurately predict both CO_2 adsorption and catalytic activity (R^2 = 0.92). Notably, the physical interpretation of these data-driven descriptors provides quantitative validation of our mechanistic insights, reaffirming the synergistic Si−Fe mechanism and, most importantly, the primary role of the Si site in governing the overall reaction. This work provides a conceptual framework for understanding and designing the next generation of complex catalytic systems.

■ ASSOCIATED CONTENT

Data Availability Statement

The data that support the findings of this study are available from the corresponding authors upon reasonable request.

Supporting Information

The Supporting Information is available free of charge at https://pubs.acs.org/doi/10.1021/acs.jpclett.5c03896.

Computational details,[29−38] definitions and analysis of the electronic band descriptors, details on confinement effects, full reaction pathways and free energy diagrams, and additional charge transfer and PDOS analysis (PDF)

■ AUTHOR INFORMATION

Corresponding Author

Xinrui Cao − *Department of Physics and Fujian Provincial Key Laboratory of Theoretical and Computational Chemistry, Xiamen University, Xiamen 361005, China;* orcid.org/0000-0002-2998-8863; Email: xinruicao@xmu.edu.cn

Authors

Meijie Wang − *Department of Physics, Xiamen University, Xiamen 361005, China;* orcid.org/0009-0008-2000-5438

Yuxing Lin − *Department of Physics, Xiamen University, Xiamen 361005, China*

Yaowei Xiang − *Department of Physics, Xiamen University, Xiamen 361005, China*

Yang Sun − *Department of Physics, Xiamen University, Xiamen 361005, China;* orcid.org/0000-0002-4344-2920

Zi-zhong Zhu − *Department of Physics, Xiamen University, Xiamen 361005, China;* orcid.org/0000-0001-5353-4418

Shunqing Wu − *Department of Physics, Xiamen University, Xiamen 361005, China;* orcid.org/0000-0002-2545-0054

Complete contact information is available at: https://pubs.acs.org/10.1021/acs.jpclett.5c03896

Author Contributions

Meijie Wang: investigation, data curation, writing-original draft, visualization; Yuxing Lin and Yaowei Xiang: formal analysis; Yang Sun, Shunqing Wu and Zi-Zhong Zhu: writing, review, and editing; Xinrui Cao: conceptualization, supervision, writing-review editing.

Notes

The authors declare no competing financial interest.

https://doi.org/10.1021/acs.jpclett.5c03896
J. Phys. Chem. Lett. 2026, 17, 1227−1234

■ ACKNOWLEDGMENTS

This work is supported by National Natural Science Foundation of China (22073076 and 21933009) and the Fundamental Research Funds for the Central Universities of China (20720240138). The Xiamen University's High-Performance Computing Center and the State Key Laboratory Chemistry of Solid Surfaces at the Xiamen University are acknowledged for the supercomputer resources. Shaorong Fang and Tianfu Wu from Information and Network Center of Xiamen University are acknowledged for the help with the GPU computing.

■ REFERENCES

(1) Burkart, M. D.; Hazari, N.; Tway, C. L.; Zeitler, E. L. Opportunities and challenges for catalysis in carbon dioxide utilization. *ACS Catal.* **2019**, *9*, 7937−7956.
(2) Johnson, D.; Qiao, Z.; Djire, A. Progress and challenges of carbon dioxide reduction reaction on transition metal based electrocatalysts. *Materials* **2021**, *4*, 8661−8684.
(3) Francke, R.; Schille, B.; Roemelt, M. Homogeneously catalyzed electroreduction of carbon dioxide-methods, mechanisms, and catalysts. *Chem. Rev.* **2018**, *118*, 4631−4701.
(4) Wu, J.; Sharifi, T.; Gao, Y.; Zhang, T.; Ajayan, P. M. Emerging carbon-based heterogeneous catalysts for electrochemical reduction of carbon dioxide into value-added chemicals. *Adv. Mater.* **2019**, *31*, 1804257.
(5) Li, M.; Wang, H.; Luo, W.; Sherrell, P. C.; Chen, J.; Yang, J. Heterogeneous single-atom catalysts for electrochemical CO_2 reduction reaction. *Adv. Mater.* **2020**, *32*, 2001848.
(6) Han, J.; Bai, X.; Xu, X.; Bai, X.; Husile, A.; Zhang, S.; Qi, L.; Guan, J. Advances and challenges in the electrochemical reduction of carbon dioxide. *Chemical Science* **2024**, *15*, 7870−7907.
(7) Dal Mas, R.; Somoza-Tornos, A.; Pérez-Fortes, M.; Kortlever, R.; Kiss, A. A. Challenges and opportunities for CO_2 electroreduction from a process systems engineering perspective. *Frontiers in Energy Research* **2024**, *12*, 1340622.
(8) Wang, A.; Li, J.; Zhang, T. Heterogeneous Single-Atom Catalysis. *Nature Reviews Chemistry* **2018**, *2*, 65−81.
(9) Cui, X.; Li, W.; Ryabchuk, P.; Junge, K.; Beller, M. Bridging Homogeneous and Heterogeneous Catalysis by Heterogeneous Single-Metal-Site Catalysts. *Nature Catalysis* **2018**, *1*, 385−397.
(10) Liu, J. Catalysis by Supported Single Metal Atoms. *ACS Catal.* **2017**, *7*, 34−59.
(11) Ren, W.; Tan, X.; Yang, W.; Jia, C.; Xu, S.; Wang, K.; Smith, S. C.; Zhao, C. Isolated diatomic Ni-Fe metal-nitrogen sites for synergistic electroreduction of CO_2. *Angew. Chem., Int. Ed.* **2019**, *58*, 6972−6976.
(12) Guo, J.; Liu, H.; Li, D.; Wang, J.; Djitcheu, X.; He, D.; Zhang, Q. A minireview on the synthesis of single atom catalysts. *RSC Adv.* **2022**, *12*, 9373−9394.
(13) Li, L.; Yuan, K.; Chen, Y. Breaking the scaling relationship limit: from single-atom to dual-atom catalysts. *Accounts of Materials Research* **2022**, *3*, 584−596.
(14) Brea, C.; Hu, G. Dual-atom catalysts for the oxygen reduction reaction: unraveling atomic structures under reaction conditions. *J. Am. Chem. Soc.* **2025**, *147*, 19210−19216.
(15) Wang, M.; Xiang, Y.; Chen, W.; Wu, S.; Zhu, Z.-Z.; Cao, X. $SiFeN_6$-graphene: a promising dual-atom catalyst for enhanced CO_2-to-CH_4 conversion. *Appl. Surf. Sci.* **2024**, *643*, 158724.
(16) Wang, M.; Xiang, Y.; Lin, Y.; Sun, Y.; Zhu, Z.-z.; Wu, S.; Cao, X. P−d orbital coupling in silicon-based dual-atom catalysts for enhanced CO_2 reduction: insight into electron regulation of active center and coordination atoms. *Journal of Materials Chemistry A* **2024**, *12*, 31902−31913.
(17) Han, G.; Zhang, X.; Liu, W.; Zhang, Q.; Wang, Z.; Cheng, J.; Yao, T.; Gu, L.; Du, C.; Gao, Y.; Yin, G. Substrate strain tunes operando geometric distortion and oxygen reduction activity of CuN_2C_2 single-atom sites. *Nat. Commun.* **2021**, *12*, 6335.
(18) Tang, S.; Xu, L.; Dong, K.; Wang, Q.; Zeng, J.; Huang, X.; Li, H.; Xia, L.; Wang, L. Curvature effect on graphene-based Co/Ni single-atom catalysts. *Appl. Surf. Sci.* **2023**, *615*, 156357.
(19) Zhang, T.; Ye, Q.; Liu, Y.; Liu, Q.; Han, Z.; Wu, D.; Chen, Z.; Li, Y.; Fan, H. J. Data-driven discovery of biaxially strained single atoms array for hydrogen production. *Nat. Commun.* **2025**, *16*, 3644.
(20) Chen, C.; Zhang, Z.; Dai, L.; Li, B.; Li, Z. High-curvature single-atom catalysts for electrocatalysis: a review. *Applied Catalysis A: General* **2025**, *694*, 120160.
(21) Zhao, Y.; et al. Acidic Oxygen Reduction by Single-Atom Fe Catalysts on Curved Supports. *Nature* **2025**, *644*, 668−675.
(22) Lin, W.; Di Tommaso, D. Screening Nitrogen-Coordinated Single Atom Catalysts on Armchair Carbon Nanotubes for Enhanced Electrochemical CO_2 Reduction to C_1 Products. *ACS Catal.* **2025**, *15*, 16463−16475.
(23) Cepitis, R.; Kongi, N.; Rossmeisl, J.; Ivanistsev, V. Vladislav Ivaništšev Surface curvature effect on dual-atom site oxygen electrocatalysis. *ACS Energy Letters* **2023**, *8*, 1330−1335.
(24) Sui, H.; Guo, Q.; Xiang, M.; Kong, X.; Zhang, J.; Ding, S.; Su, Y. Theoretical insights of curvature effects of FeN_4-doped carbon nanotubes on ORR activity. *J. Phys. Chem. Lett.* **2024**, *15*, 8257−8264.
(25) Mustonen, K.; Laiho, P.; Kaskela, A.; Zhu, Z.; Reynaud, O.; Houbenov, N.; Tian, Y.; Susi, T.; Jiang, H.; Nasibulin, A. G.; Kauppinen, E. I. Gas phase synthesis of non-bundled, small diameter single-walled carbon nanotubes with near-armchair chiralities. *Appl. Phys. Lett.* **2015**, *107*, 013106.
(26) Dronskowski, R.; Bloechl, P. E. Crystal orbital Hamilton populations (COHP): energy-resolved visualization of chemical bonding in solids based on density-functional calculations. *J. Phys. Chem.* **1993**, *97*, 8617−8624.
(27) Deringer, V. L.; Tchougréeff, A. L.; Dronskowski, R. Crystal Orbital Hamilton Population (COHP) Analysis As Projected from Plane-Wave Basis Sets. *J. Phys. Chem. A* **2011**, *115*, 5461−5466.
(28) Ouyang, R.; Curtarolo, S.; Ahmetcik, E.; Scheffler, M.; Ghiringhelli, L. M. SISSO: a compressed-sensing method for identifying the best low-dimensional descriptor in an immensity of offered candidates. *Physical Review Materials* **2018**, *2*, 083802.
(29) Kresse, G.; Furthmüller, J. Efficient iterative schemes for ab initio total-energy calculations using a plane-wave basis set. *Phys. Rev. B* **1996**, *54*, 11169−11186.
(30) Kresse, G.; Furthmüller, J. Efficiency of ab-initio total energy calculations for metals and semiconductors using a plane-wave basis set. *Comput. Mater. Sci.* **1996**, *6*, 15−50.
(31) Blöchl, P. E. Projector augmented-wave method. *Phys. Rev. B* **1994**, *50*, 17953−17979.
(32) Perdew, J. P.; Burke, K.; Ernzerhof, M. Generalized gradient approximation made simple. *Phys. Rev. Lett.* **1996**, *77*, 3865−3868.
(33) Grimme, S.; Antony, J.; Ehrlich, S.; Krieg, H. A consistent and accurate ab initio parametrization of density functional dispersion correction (DFT-D) for the 94 elements H-Pu. *J. Chem. Phys.* **2010**, *132*, 154104.
(34) Grimme, S.; Ehrlich, S.; Goerigk, L. Effect of the damping function in dispersion corrected density functional theory. *J. Comput. Chem.* **2011**, *32*, 1456−1465.
(35) Wang, V.; Xu, N.; Liu, J.-C.; Tang, G.; Geng, W.-T. VASPKIT: a user-friendly interface facilitating high-throughput computing and analysis using VASP code. *Comput. Phys. Commun.* **2021**, *267*, 108033.
(36) Sundararaman, R.; Letchworth-Weaver, K.; Schwarz, K. A.; Gunceler, D.; Ozhabes, Y.; Arias, T. JDFTx: software for joint density-functional theory. *SoftwareX* **2017**, *6*, 278−284.
(37) Kim, D.; Shi, J.; Liu, Y. Substantial impact of charge on electrochemical reactions of two-dimensional materials. *J. Am. Chem. Soc.* **2018**, *140*, 9127−9131.
(38) Garrity, K. F.; Bennett, J. W.; Rabe, K. M.; Vanderbilt, D. Pseudopotentials for high-throughput DFT calculations. *Comput. Mater. Sci.* **2014**, *81*, 446−452.

https://doi.org/10.1021/acs.jpclett.5c03896
J. Phys. Chem. Lett. 2026, 17, 1227−1234